European Polymer Journal 68 (2015) 190–206

Contents lists available at ScienceDirect

European Polymer Journal

journal homepage: www.elsevier.com/locate/europolj

Macromolecular Nanotechnology

The improvement of mechanical performance and water-response of carboxylated SBR by chitin nanocrystals

Mingxian Liu *, Qi Peng, Binghong Luo, Changren Zhou *

Department of Materials Science and Engineering, Jinan University, Guangzhou 510632, PR China

ARTICLE INFO

Article history:
Received 19 February 2015
Received in revised form 23 April 2015
Accepted 26 April 2015
Available online 27 April 2015

Keywords:
Chitin nanocrystals
Mechanical properties
Rubber
Dispersion

ABSTRACT

Carboxylated styrene-butadiene rubber (xSBR) composites with chitin nanocrystals (CNCs) were prepared by solution-casting method. CNCs prepared by acid hydrolysis show rod-like morphology with diameter of ~15 nm and length of 200–500 nm. The hydrogen bonding interactions between the rubber and CNCs are confirmed by FTIR. Tensile testing demonstrates CNCs can significantly increase the tensile strength, tensile modulus, and strain at break of xSBR. The dispersion of CNCs is homogenous in the matrix even at high loadings. The storage moduli (E') of the composites increase by CNCs especially at rubber region. The glass transition temperature of xSBR nearly does not change after the incorporation of CNCs. Upon submersion in deionized water, dramatic reduction of tensile modulus is observed for the nanocomposites, for example, from 31.1 to 2.8 MPa for nanocomposite containing 3 wt.% CNCs. These changes are interpreted as the formation of percolating CNCs network and the interfacial interactions in the composites.

1. Introduction

Polymers reinforced by renewable polysaccharide nanocrystals such as cellulose, chitin and starch, have attracted great attentions in recent years owing to their advantages over inorganics filled polymer composites [1–5]. The main advantages of polymer composite containing polysaccharide nanocrystals are low density, high mechanical properties, biocompatibility, biodegradability, and stimuli-responsive property brought by the nanocrystals [6]. For example, rigid cellulose nanofiber was incorporated into rubbery ethylene oxide-epichlorohydrin copolymer (EO-EPI) [7], poly(vinyl acetate) (PVAc) [8,9], or polyurethane (PU) [10], which mimicked the sea cucumber dermis architecture and accommodated the uptake of several chemical stimuli. The nanocomposites exhibit a reversible reduction by a factor of 40 of the tensile modulus upon exposure to a chemical regulator that mediates nanocrystals interactions [7]. Starch nanocrystals have also been introduced into different polymers for the preparation of nanocomposites [6]. For preparing the nanocrystals reinforced polymer nanocomposites, an aqueous dispersion of the nanocrystals should be prepared by acid hydrolysis of biomass which removes the disordered and low lateral ordered crystalline defects. Afterwards, the homogeneous dispersion of these nanocrystals within a polymeric matrix should be achieved by ultrasonic treatment. The final nanocomposite in the form of film [11,12], gel, fiber [13], or porous scaffold [14] can be obtained after removing the water medium.

As for polysaccharide nanocrystals used in polymer composites, most researchers have focused on cellulose and starch, but the attempts to use chitin nanocrystals (CNCs) have been rarely reported. As the second most abundant biopolymer after

* Corresponding authors.
E-mail addresses: liumx@jnu.edu.cn (M. Liu), tcrz9@jnu.edu.cn (C. Zhou).

http://dx.doi.org/10.1016/j.eurpolymj.2015.04.035
0014-3057/

cellulose, chitin is strategic importance given its many excellent properties including biocompatibility, biodegradability, nontoxicity, absorption properties, and so on [15]. Chitin has many applications in variety of areas such as biomedical engineering, agriculture, water treatment, and cosmetics. Chitin occurs in nature as ordered crystalline microfibrils which act as structural components in the exoskeleton of arthropods and in the cell walls of fungi and yeast. Similarly to cellulose nanocrystals, some crystalline particles can be isolated by acid hydrolysis [16]. Marchessault et al. firstly reported a route for preparing suspension of chitin crystallite particles and their liquid crystals formation ability [17]. The large surface area and high Young's modulus make CNCs ideal candidates as fillers in polymer nanocomposites.

Both natural and synthetic polymers, including rubbers [18–20], thermoplastics [21,22], water-soluble polymers [11,12], have been mixed with CNCs for improving the mechanical properties. From the year of 2000, Dufresne et al. prepared crab shell chitin whisker reinforced natural rubber (NR) [18–20], poly(caprolactone) (PCL) [23], poly(styrene-co-butyl acrylate) (poly(S-co-BuA)) [21] nanocomposites either by freeze-drying and hot-pressing or by casting and evaporating. The formation of three-dimensional filler networks in the polymer matrix and its effect on the swelling behavior and mechanical properties were investigated in detail. They also studied the influence of the chemical modification of the CNCs on the reinforcing ability of the NR matrix [20]. Carboxylated styrene-butadiene rubber (xSBR)/chitin microsized particles composites were also prepared in a similar way [24]. All these results suggest a direct relationship between the filler network and the properties improvement. Zhang et al. found the tensile properties and water resistance of the soy protein isolate (SPI) plastics increased by the incorporation of the CNCs [22]. Due to the hydrophilcity of the chitin, the CNCs are easily dispersed in water-soluble polymer matrix by solution mixing method. For example, fibers of poly(-vinyl alcohol) (PVA)/CNCs were prepared by gel spinning and the resulted composite fibers exhibited the enhancement in mechanical and anti-creep properties [13]. The silk fibroin/CNCs nanocomposite sponges prepared by solution mixing and freeze-drying technique also show improved mechanical property and good biocompatibility. The polymer nanocomposite films reinforced by CNCs, including chitosan [12], PVA [11], xyloglucan [25], have also been studied. Recently, the surface modified CNCs were employed as multifunctional crosslinkers for the preparation of polyacrylamide nanocomposite hydrogels [26].

Since there have not prior reports on the preparation and the properties of xSBR nanocomposites with nanosized chitin, the CNCs were firstly prepared by acid hydrolysis of chitin in the present contribution. Nanocomposite films using the obtained CNCs as nanofillers were prepared by solution casting from mixtures of xSBR latex and CNCs dispersion. xSBR was chosen as the polymer matrix material, due to its excellent film-forming ability, high hydrophilicity, and good transparency [27]. xSBR has wide applications in adhesive for paper and printing industry [28]. However, the low strength and modulus limits xSBR practical applications. Consequently, CNCs is expected to improve the mechanical properties of the resulting xSBR nanocomposite films. The formation of the percolation network of CNCs and the stimuli-responsive mechanical properties of the nanocomposite are investigated.

2. Experimental

2.1. Materials

Chitin powder (K1262) was purchased from Sanland-chem International Inc. and used without further purification. The degree of acetylation (DA) of the chitin was determined by elemental analysis to be 0.98%. xSBR latex, with solid content of 50%, was purchased from Guangzhou Juntai Materials Co. Ltd. The xSBR is a copolymer of styrene, butadiene, acrylic acid and the chemical structure of xSBR is shown below. Water was purified by deionization and filtration with a Millipore purification apparatus (resistivity > 18.2 MΩ cm). Hydrochloric acid (HCl) (37% w/w) was of analytical grade and used without further purification.

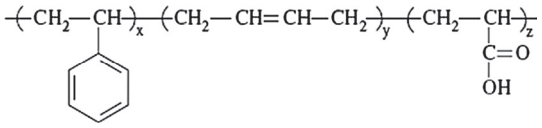

Chemical structure of xSBR (x/y/z=42.0/56.4/1.6)

2.2. Preparation of chitin nanocrystals (CNCs)

Chitin nanocrystals (CNCs) were prepared from chitin powder based on the method of Marchessault et al. [17]. The nanocrystals dispersion was prepared by hydrolyzing chitin with 3 N HCl at its boiling point (i.e. 104°C) for 90 min under vigorous stirring. The ratio of 3 N HCl to chitin was 30 mL g^{-1}. After acid hydrolysis, the suspensions were diluted with distilled water, followed by centrifugation at 4000 rpm for 10 min. This process was repeated three times to remove the excessive acid and the amorphous phase. The suspensions were then transferred to a dialysis bag and dialyzed in running water for 2 h and later in distilled water overnight. The complete nano-dispersion of CNCs in aqueous suspension at the individual fibril level was achieved by ultrasonic treatment using JY99-IIDN ultrasonic cell disruptor (Ningbo scientz company, China)

at 800 W for 1 h. The morphology of CNCs was observed with a ZEISS, Ultra55 SEM machine, Philips Tecnai 10 transmission electron microscopy (TEM) machine, and a multimode AFM with NanoScope IIIa controller (Veeco Instruments). The sample for SEM analysis was prepared by dropping of the 0.025 wt.% CNCs dispersion on clean mica plate and subsequently freeze-dried at −80 °C. The particle size distribution and Zeta-potential of CNCs aqueous dispersion (0.01 wt.%) was measured with a Zetasizer Nano ZS (Malvern Ltd., UK).

2.3. Preparation of xSBR-CNCs nanocomposites

The xSBR-CNCs nanocomposite films were prepared by solution-casting method. The typical procedures were shown as follows. The CNCs nano-dispersion was prepared by ultrasonic treatment of freeze-dried CNCs. Varying amount of the CNCs dispersions were then added to the xSBR latex (with appropriate addition of distilled water to obtained 100 g of the final dispersion) to achieve the nanocomposite films with nanocrystals content in the range of 0–5 wt.%. The xSBR/CNCs mixture dispersion was further stirred mechanically for another 6 h and vacuum degassing before being cast onto a polytetrafluoroethylene (PTFE) mold. The solvent was evaporated at 40 °C for 12 h in a convection oven then at 60 °C under vacuum for 2 h. The obtained CNCs-reinforced xSBR nanocomposite films were stored in desiccator when not in use.

2.4. Characterizations

2.4.1. Light transmittances

The light transmittances of the neat xSBR and xSBR/CNCs nanocomposites films with ~0.30 mm thickness were measured from 200 to 1000 nm using a UV-1800 (Shanghai Yoke Instrument Co., Ltd., China) UV–vis spectrometer.

2.4.2. Fourier transform infrared spectroscopy (FTIR)

The FTIR spectra of neat xSBR and xSBR/CNCs nanocomposites films were measured using attenuated total reflectance (ATR) model in a Bruker FTIR. Thirty-two consecutive scans were taken and their average was stored. Spectra were taken from 4000 to 400 cm^{-1}. The resolution of the wavenumber was 2 cm^{-1}.

2.4.3. Mechanical properties determination

The neat xSBR and xSBR/CNCs nanocomposite films were cut into the dog-bone shape with width and thickness of 6 mm * 0.3 mm. Then the samples were stretched at 50 mm/min rate using the SHIMADZU AG-1 machine. The stress–strain curves for every sample were recorded. The value of the Young's modulus was obtained in the strain range of 0.1–0.25%. And the data was automatically given by the TRAPEZIUMX software. The modulus at 100% or 300% strain of the sample was the stress required to produce 100% or 300% elongation (strain).To determine the water response of the mechanical property of the xSBR/CNCs nanocomposites, the samples were immersed into 80 mL water for 3 days under room temperature and then performed the testing immediately with a similar procedure. At least five specimens for every sample were tested for reliable data.

2.4.4. Dynamic mechanical analysis (DMA)

Dynamic mechanical analyses of neat xSBR and xSBR/CNCs nanocomposite films were conducted with a TA Q800 at an oscillation frequency and heating rate of 1.0 Hz and 3 °C/min, respectively. The tensile mode was selected and the experiment was conducted at a temperature range of -100~100 °C under nitrogen atmosphere.

2.4.5. X-ray diffraction (XRD)

XRD profiles of the chitin powder, CNCs, xSBR/CNCs nanocomposite films were obtained using X-ray diffractometer (Rigaku, MiniFlex600, CuKα, Japan) at room temperature. The scanning angle was from 5° to 60°.

2.4.6. Scanning electron microscopy (SEM)

The cross section of the cryofractured surface of the composite films was plated with a thin layer of gold before the observations. The SEM observations were done using a ZEISS, Ultra55 SEM machine.

2.4.7. Transmission electron microscopy (TEM)

Ultrathin sections (200 nm) of the rubber samples were cut using an ultramicrotome (EM ULTRACUT UC, Leica) and the sections were supported by a perforated carbon film on Cu grids. TEM analysis of the nanocomposites was carried out with a Philips Tecnai 12 TEM at an accelerating voltage of 100 kV.

2.4.8. Swelling behavior in water and toluene

The degree of aqueous swelling of neat xSBR and xSBR/CNCs nanocomposite films was gravimetrically determined by measuring the weight of samples pre- and post swelling in deionized water under room temperature for 2 days. The swelling ratios were calculated according to the following equation.

$$\text{swelling ratio} = \frac{\text{mass of wet sample} - \text{mass of dry sample}}{\text{mass of dry sample}} \times 100\%$$

The fraction of the rubber bonded to the CNCs and the fraction of rubber dissolved in toluene were estimated. Thin disks of sample materials were first weighed (M_0) and then immersed in toluene under room temperature for 72 h. They were subsequently dried for 12 h at 60 °C and weighed again (M_0'). The relative weight loss (RWL) was calculated according to the following equation.

$$\text{Relative weight loss (RWL)} = \frac{M_0 - M_0'}{M_0} \times 100\%$$

2.4.9. Contact angle measurement

Water contact angles of the rubber surfaces were measured with KRUSS Drop Shape Analyzer DSA 100 instrument under room temperature. The data measurement was repeated for five times to obtain reliable values. The volume of water droplet was 4 μL for the contact angles measurement. The contact angles were calculated by software according to the Laplace–Young model.

3. Results and discussion

3.1. Characterizations of the CNCs

The prepared CNCs suspensions via acid hydrolysis are opaque (Fig. 1a), suggesting that significant amounts of fibril bundles or unfibrillated fractions, the sizes of which are comparable to or larger than wavelengths of visible light, are present in the suspensions [29]. Thus, complete nano-dispersion of chitins at the individual fibril level should be achieved by further treatment. The appearance of the CNCs dispersion after strongly ultrasonic treatment becomes transparent (Fig. 1b), indicating the complete exfoliation of the chitin nanofibers. The positively charged character (NH^{3+}) at the surface of the nanocrystals, resulting from the protonation of amino groups, leads to the highly dispersed dispersion. The nanocrystals dispersion is

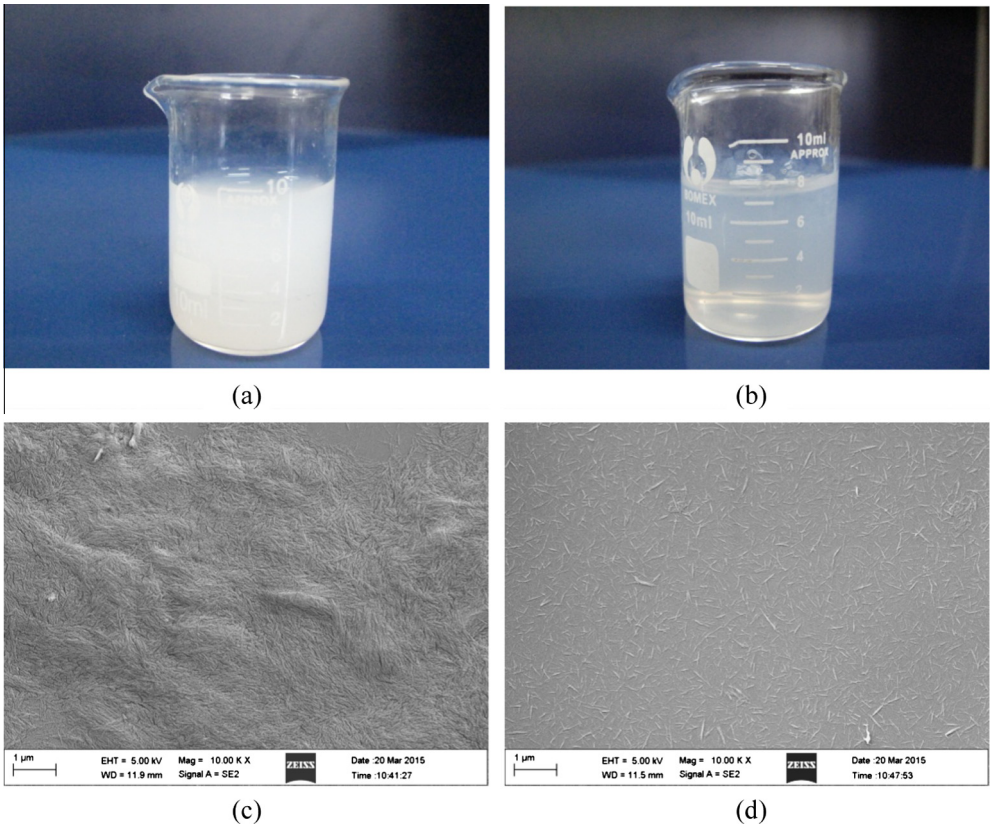

Fig. 1. The appearance and SEM morphology of CNCs aqueous suspension before ((a) and (c)) and after ((b) and (d)) ultrasonic treatment. The samples for SEM analysis were prepared by freeze-drying the corresponding suspension above.

stable for several months without sedimentation. The morphology of the dried CNCs dispersion before and after ultrasonic treatment was observed by SEM. It can be seen that the aggregated CNCs completely exfoliate into nanofibers by strongly ultrasonic treatment (Fig. 1d). The stability of aqueous CNCs dispersion is mainly contributed by their hydrophilicity and electrostatic repulsion of positively-charged acetyl groups [30]. The zeta potential is an important parameter in the examination of the stability of the nanocrystal dispersions in aqueous media. The zeta potential of the prepared CNCs dispersion is determined as +37.9 mV.

The prepared CNCs dispersion shows a Tyndall effect which is the typical character of colloid systems (Fig. 2a). The morphology of the prepared CNCs is further investigated by the SEM and TEM (Fig. 2b and c). The CNCs exhibit a rod-like morphology with average width of 15 nm, length of 200–500 nm, and aspect ratio of 13–33, as established by SEM and TEM photos. The present morphology result of CNCs is similar with that of previous reported polysaccharide nanocrsytals [29,31]. The particle size distribution of CNCs shows that they have a narrow size distribution with mean diameter of 55 nm (Fig. 2d). The particle size of CNCs ranges from 30 to 200 nm. It should be noted that the dimension of the CNCs determined by laser particle size analyzer is different from that determined by the SEM or TEM techniques. This is due to the different principal of the determining for the two techniques. The laser particle size analyzer base on light scatting is more propitiate for the spherical particles. The features of the nanosized chitin indicate their potential applications in polymer nanocomposites.

AFM technique was further employed to study the morphology of the prepared CNCs. Fig. 3 shows the height and 3D image of CNCs. AFM images of the CNCs have higher resolutions than TEM images. It is clearly seen that the CNCs have uniformly dispersed morphology with rod-like microstructure. The CNCs height determined from the AFM images are 5–15 nm, which is in good agreement with those observed from SEM and TEM images above. The width of CNCs determined from Figs. 3e and 3f is 48.5 ± 5.3 nm. Nearly no aggregates have been found in the CNCs samples, indicating their good dispersion state in their aqueous dispersion. Therefore, CNCs is ideal nanofiller component for preparing water-soluble polymer nanocomposites.

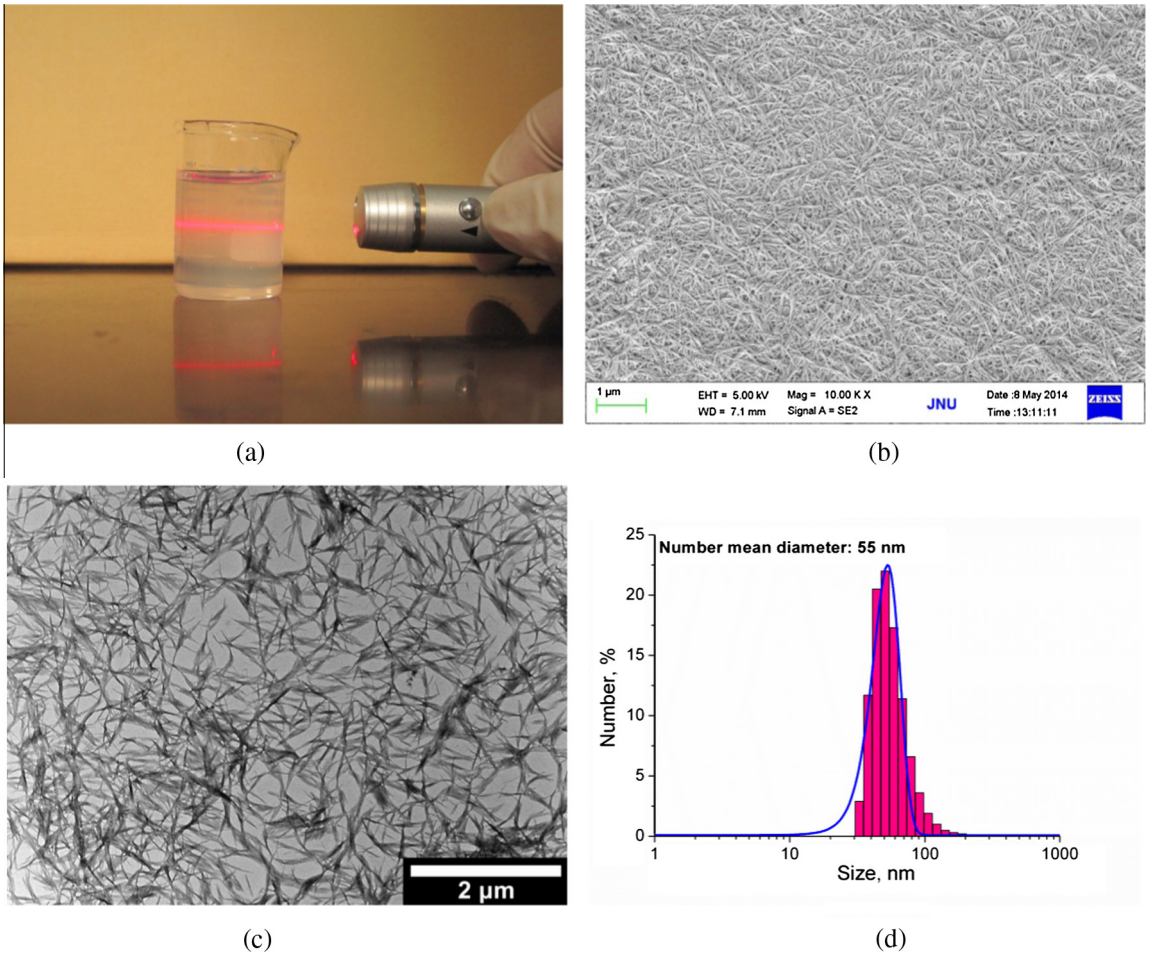

Fig. 2. The formation of light beam for the CNCs dispersion (a); SEM (b) and TEM (c) photo of the CNCs; and particle size distribution of the CNCs determined by the laser particle size analyzer (d).

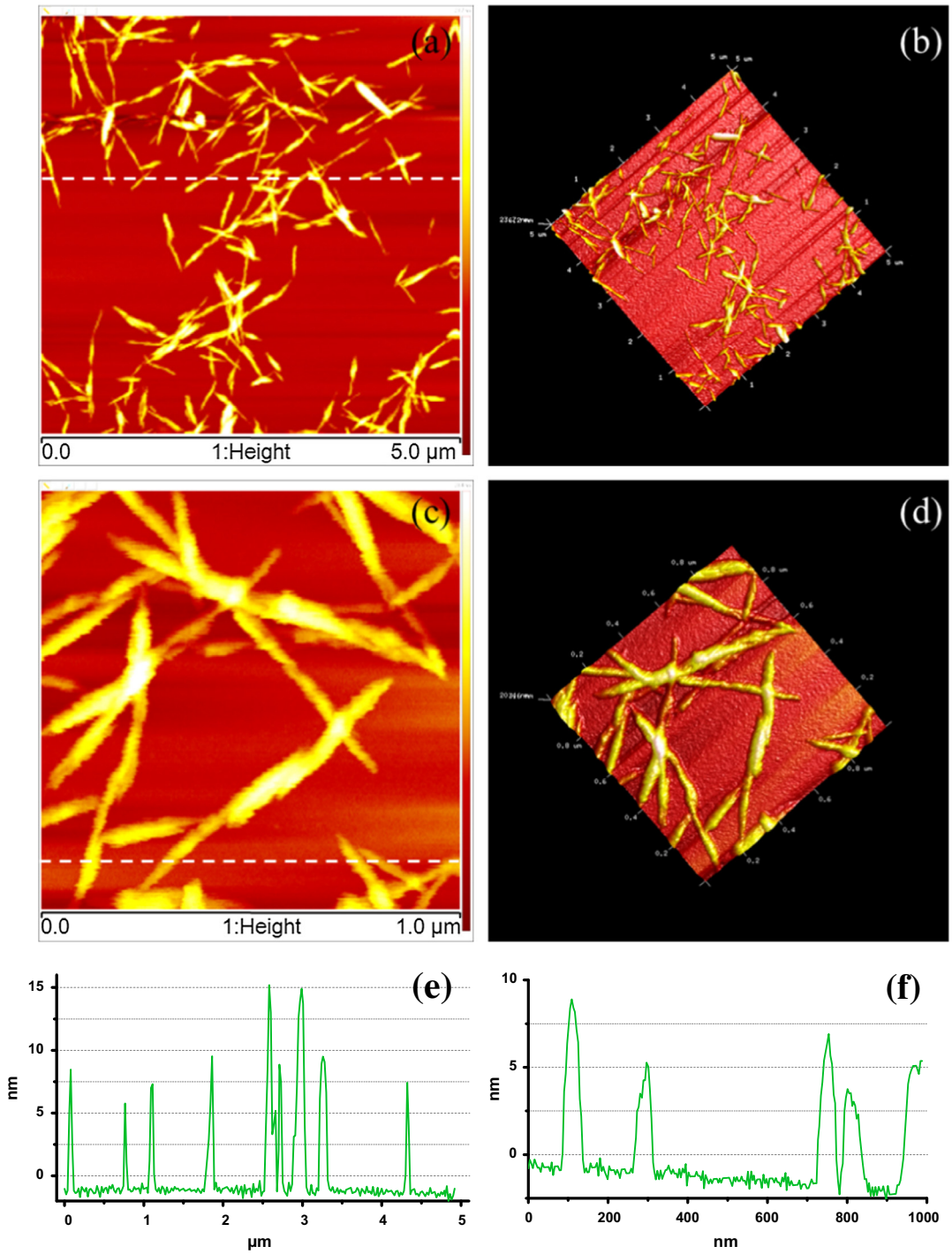

Fig. 3. AFM height ((a) and (c)) and, 3D image ((b) and (d)), and the corresponding profiles ((e) and (f)) of CNCs.

3.2. Appearance and the interfacial interactions of the xSBR/CNCs nanocomposites

Using the solution mixing method, xSBR/CNCs nanocomposites with 0–5 wt.% CNCs loading were successfully prepared. The easiest way to assess the dispersion of the nanocrystals within the host polymeric matrix is a simple examination with the naked eye [32]. Addition of a microscaled filler to a transparent polymers usually results in a loss of transparency, while

polymer nanocomposite films containing nanoscale particles remain transparent. The appearance of the neat xSBR and xSBR/CNCs nanocomposite is shown in Fig. 4(a). It can be seen that all the films are transparent even the thickness of the films is ~300 μm. The light transmittances were determined by UV–vis spectrophotometer as shown in Fig. 4(b). It can be seen that the light transmittances is slightly decreased due to the addition of CNCs. In the visible light wavelength range (400–760 nm), the maximum reduction value of the transmittances of the nanocomposite is 6.5% compared with that of pure xSBR film. No aggregated CNCs can be observed in the nanocomposite films by naked eyes. This is attributed to that the complete nano-dispersion is achieved by ultrasonic treatment of the CNCs suspension and subsequent in xSBR matrix. The homogenous dispersion of nanofillers is benefit for the improvement of mechanical and thermal performance of the rubber nanocomposites.

The interfacial interaction between fillers and polymer matrix is one of critical factors determining the property improvement of composite. FTIR spectra were obtained for the CNCs powder, neat xSBR, and xSBR-CNCs model compound (weight ratio, 1:1) (Fig. 5) to investigate the interfacial interactions. The spectrum of neat xSBR shows characteristic bands at approximately 3358 cm^{-1} (O—H stretching), 1728 cm^{-1} (C═O of carboxyl group), 967 cm^{-1} (1,4 trans butadiene units), 909 cm^{-1} (1,2 vinyl), 757 cm^{-1} (1,4 cis), and 699 cm^{-1} (styrene units) [33]. Also, the IR peaks of present prepared CNCs are consistent with the spectrum of previous reported one [34]. For example, they show peak around 3450 cm^{-1} (hydrogen-bonded OH groups) and 1624 cm^{-1} (C═O groups hydrogen-bonded OH groups), which are the characteristic peaks of α-chitin. The structure change of xSBR-CNCs nanocomposite is mostly observed from the change in the amide-I (1658 cm^{-1}) and amide-II (1558 cm^{-1}) bands of chitin. The amide I (C═O stretching) split peaks at 1658 cm^{-1} and 1627 cm^{-1} which are attributed to the hydrogen bonding of the C═O group of chitin to the —NH group of an adjacent chitin chain (1657 cm^{-1}) and with an —OH group on the same chitin chain (1620 cm^{-1}) [35]. In the xSBR/CNCs nanocomposites, the amide I band shifts to lower wavenumber, indicating the additional hydrogen bonding between the C═O of chitin and the hydroxyl groups of xSBR. Further indication of the CNCs-xSBR hydrogen bonding is gathered from the shift of the amide II band (1558 cm^{-1}) in the composite. Amide II band in chitin corresponds to the —NH bending and stretching modes mixed with the —CN stretching mode. In total, this FTIR data confirm a strong hydrogen bonding interactions between CNCs and xSBR in the composite, although the exact structural nature of the bond will require further investigation. The interfacial interactions are critical to property improvement of the polymer nanocomposites, which will be shown as below.

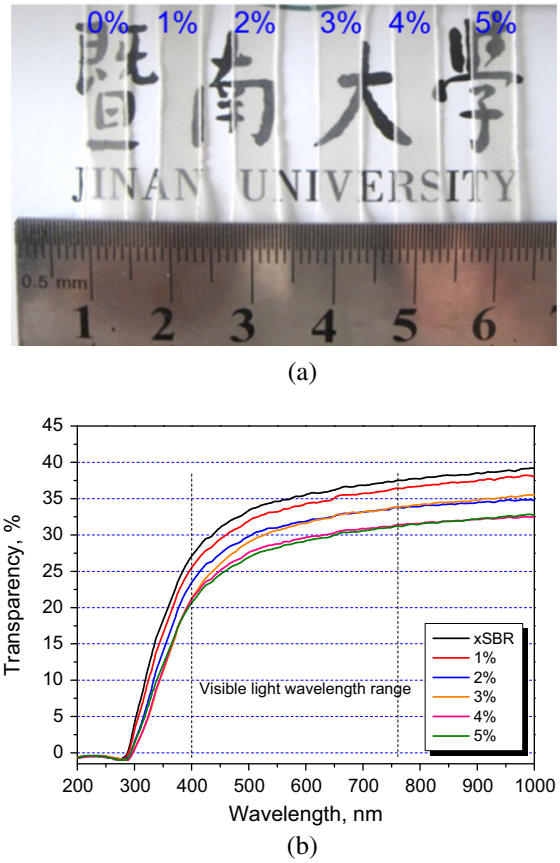

Fig. 4. Appearance (a) and the UV–vis light transmittances (b) of xSBR/CNCs nanocomposites with different CNCs contents.

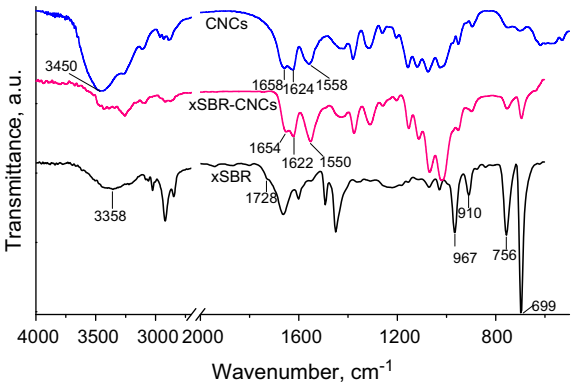

Fig. 5. FTIR spectra of xSBR, chitin nanocrystals and xSBR-chitin model compound.

3.3. Mechanical properties of the xSBR/CNCs nanocomposites

Nanoscale dimensions and impressive mechanical properties (elastic modulus of 150 GPa [36]) of the high aspect ratio rod-like CNCs make them ideal candidates to improve the mechanical properties of the polymers. The reinforcement of CNCs on the xSBR was firstly investigated by the tensile testing. Fig. 6 shows the typical tensile stress–strain curves for the neat xSBR and xSBR/CNCs nanocomposites. Table 1 summarizes the value of the mechanical properties data of the nanocomposites. The tensile strength and elongation at break of the nanocomposites increases when the content of CNCs is lower than 4 wt.%. For example, the nanocomposite with 3 wt.% CNCs, the tensile strength and the elongation at break is 9.16 MPa and 396%, respectively, which is 2.23 folds and 11.0% higher compared with those for neat xSBR respectively. The strength increases continually (the maximum value is 10.4 MPa) by further loading of CNCs into the xSBR, but the rupture elongation decreases compared with that of neat xSBR. The small amount of CNCs act as the physical crosslinker of the xSBR and therefore enhance the mobility of the polymer chains. Overloading of the CNCs into the xSBR, they may form a stiff network in the polymer matrix which can stiffen the composites and suppress the flexibility of the rubber chains [37]. As a result, the rupture elongation of the nanocomposite decreases when the loading of CNCs is relatively high.

Fig. 7 shows the influence of CNCs loading on the modulus of xSBR nanocomposites. The elastic modulus, modulus at 100% strain and modulus at 300% strain of the composites increases dramatically with CNCs content. For xSBR nanocomposites with 5 wt.% CNCs, the elastic modulus and modulus at 100% strain increase from 14.1 MPa and 1.9 MPa to 39.2 MPa and 5.5 MPa, which are 178% and 189% higher than those of neat rubber, respectively. The outstanding reinforcement of the CNCs to the xSBR is attributed to the homogeneous dispersion of the rigid CNCs and the interfacial interactions between the rubber matrix and CNCs. In particular, the formed percolation network of the CNCs can effetely tolerate the stress from the rubber, as a result strengthening the composites significantly.

3.4. Microstructures of the xSBR/CNCs nanocomposites

The microstructures of the xSBR/CNCs nanocomposites were investigated by XRD and SEM. As shown in Fig. 8, neat xSBR exhibits a wide diffraction peak around $2\theta = 19.5°$, indicating the amorphous state of the rubber matrix. The XRD pattern of

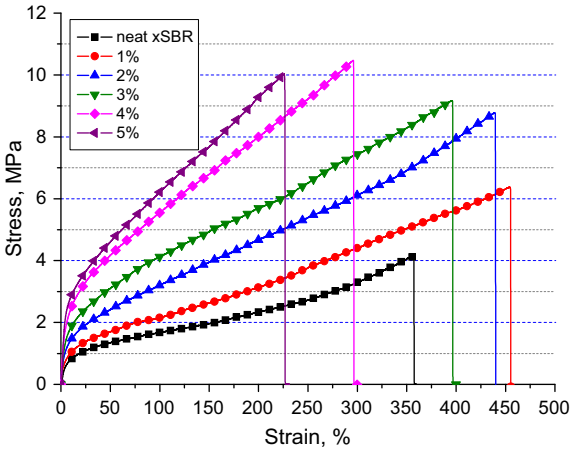

Fig. 6. The tensile stress–strain curves for xSBR and xSBR/CNCs nanocomposites.

Table 1
The mechanical properties for xSBR/CNCs nanocomposites (the data in the bracket is the standard deviation).

CNCs content (phr)	Young's Modulus (MPa)	Modulus at 100% strain (MPa)	Modulus at 300% strain (MPa)	Tensile strengths (MPa)	Elongation at break (%)
0	14.10 (1.09)	1.85 (0.18)	3.70 (0.34)	4.29 (0.45)	374.5 (21.1)
1	14.27 (1.30)	2.07 (0.06)	4.07 (0.36)	6.26 (0.51)	423.5 (31.6)
2	24.45 (1.87)	3.17 (0.05)	5.88 (0.21)	8.68 (0.35)	419.7 (19.9)
3	31.13 (1.78)	4.12 (0.01)	7.76 (0.49)	9.42 (0.26)	389.1 (17.5)
4	36.17 (1.13)	4.63 (0.26)	9.37 (0.64)	10.51 (0.44)	296.7 (21.0)
5	39.23 (0.49)	5.54 (0.24)	10.22 (0.34)	10.40 (0.34)	240.8 (32.6)

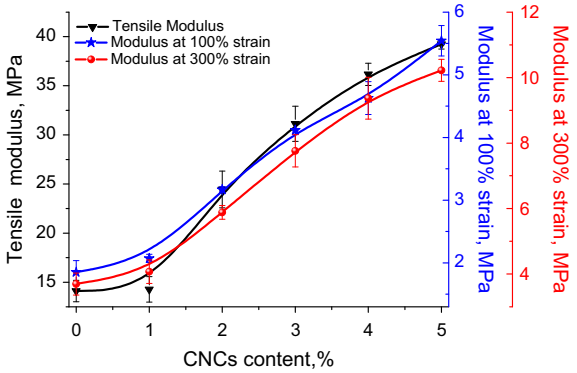

Fig. 7. The influence of CNCs loading on the modulus of xSBR nanocomposites.

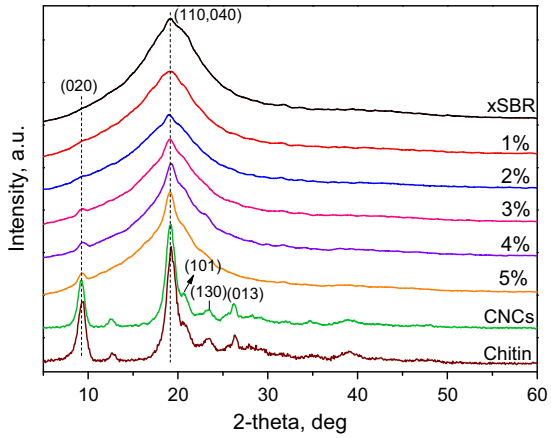

Fig. 8. The XRD patterns of raw chitin, CNCs, neat xSBR and xSBR/CNCs nanocomposites.

CNCs shows strong scattering peaks at 2θ of 9.6° (020 plane) and 19.5° (110,040 plane) as well as three other weak peaks at 21° (101 plane), 23° (130 plane) and 26° (013 plane). This is consistent with the diffraction peak of raw chitin, suggesting the acidiolysis process does not affect the crystal structure of chitin [38]. When the loading of CNCs is less 3 wt.%, there is no peak assigned to CNCs. After that, a small peak around 9.6° assigned 020 plane of CNCs gradually appears in the composite. Because the XRD pattern is statistics result, more the loading of CNCs is, larger the intensity of the peaks. The XRD results suggest CNCs are successfully incorporated into the xSBR.

SEM was used to study the morphology of xSBR/CNCs nanocomposite, and the results are shown in Fig. 9. The white points with high brightness in the SEM photos represent the CNCs. It can be seen that CNCs are uniformly dispersed in the rubber matrix nearly indecency of the CNCs loadings. With the increase of CNCs loading, the white points increases, suggesting the successful incorporation of different content of CNCs. No aggregated CNCs are found even with 4 wt.% CNCs nanocomposite. The CNCs aggregates are broken under ultrasonic treatment as shown in the AFM images. The good dispersion ability of CNCs is attributed to the rod-like morphology and the charge repulsion effects among the CNCs. The good

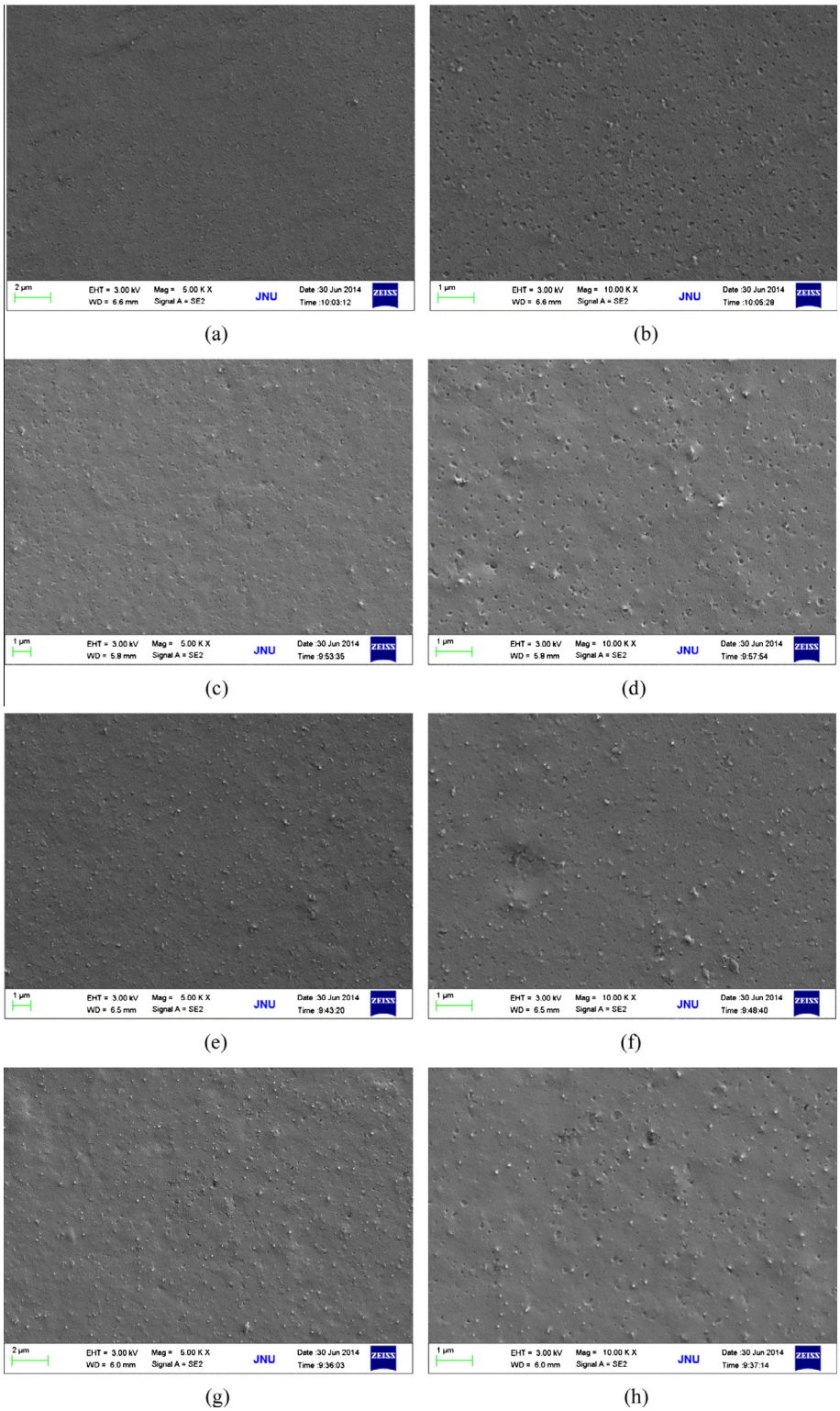

Fig. 9. The SEM photos of the fracture surface of xSBR and xSBR/CNCs composites: (a) and (b) xSBR; (c) and (d) 1%; (e) and (f) 2%; (g) and (h) 3%; (i) and (j) 4%; (k) and (l) 5%.

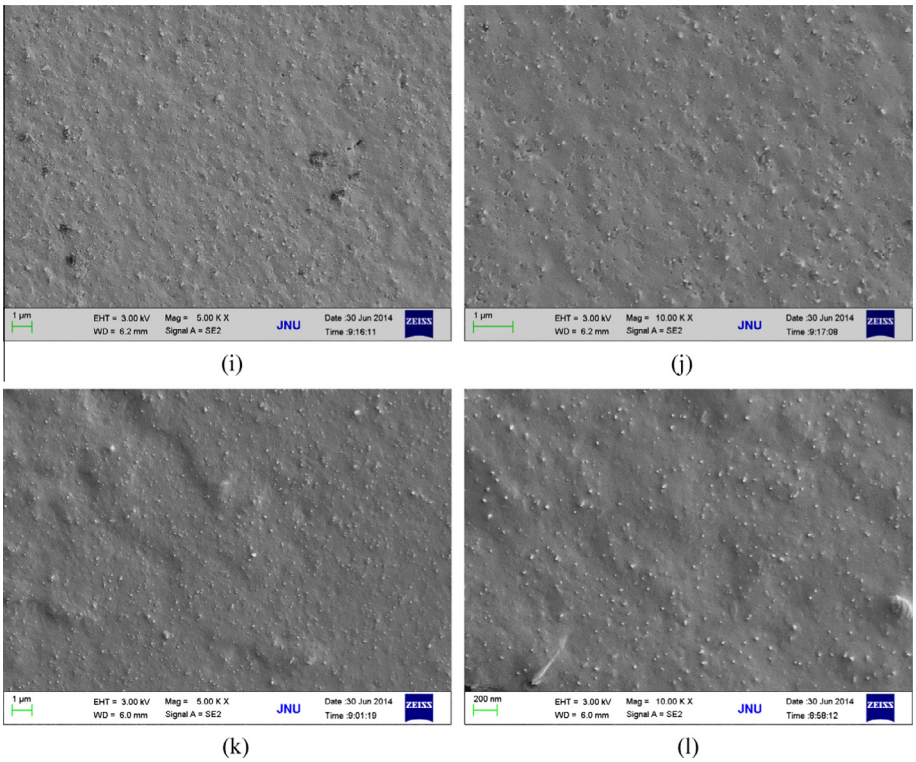

Fig. 9 (*continued*)

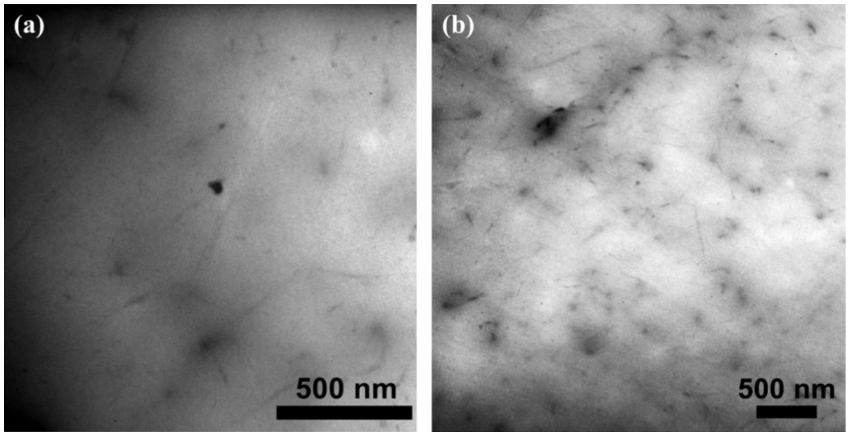

Fig. 10. TEM images of the of xSBR/CNCs composites: (a) 2% CNCs and (b) 4% CNCs.

dispersion state of CNCs in other polymer matrix, as reported in previous reports [29], is critical for the mechanical property improvement since the dispersed phase can effectively tolerate the stress and heat. However, overloading the light-weighted CNCs into the polymers leads to aggregates in polymer matrix, as the volume content of the filler are too high.

The homogenous dispersion of CNCs in the xSBR matrix was further confirmed by TEM as shown in Fig. 10. The contrast between the rubber and the nanocrystals is low due to the low atomic number elements (C, O, N) for the CNCs chemical composition [39]. It is difficult for achieving TEM images with high resolution and high contrast for this composite system. Nevertheless, well dispersed CNCs can be observed in the xSBR matrix even the loading of the CNCs is 4 wt.%. The aspect ratio of the CNCs is not changed in the composites, suggesting that the solution casting method is suitable for the preparation of CNCs reinforced polymer composites.

3.5. Dynamic mechanical and thermal properties of the xSBR/CNCs nanocomposites

The structure and properties of nanocomposites are usually relevant to the cooperative effects of many factors including the network among nanofillers, the interfacial interactions, the scale of dispersion, and the surface functionality of the nanofillers. A three-dimensional network formed by the interconnection of polysaccharide nanocrystals and stabilized by hydrogen bonding, is the predominant contributor to reinforcement of the resultant polymer nanocomposites [6]. The nanocrystals can significantly enhance the tensile strength and Young's modulus and also give a higher storage modulus, a thermally stable rubbery plateau. DMA was carried out to further examine the reinforcing effect of CNCs network on the performance of the xSBR nanocomposites under dynamic stress environment. Fig. 11 shows the temperature dependences of the storage modulus (E') and loss tangent (tan δ) for the xSBR/CNCs nanocomposites. The values of E' at −100, 30, and 80 °C, the tan δ peak values and the corresponding temperatures of the xSBR/CNCs nanocomposites are summarized in Table 2. As shown in Fig. 11(a) and Table 2, the E' of the xSBR/CNCs nanocomposites increases significantly as the CNCs concentration increases in both the rubbery region and the glassy region (except the nanocomposite with 1 wt.% CNCs). Moreover, the increasing ratios increase with the increase of temperature. For example, the values of E' for the

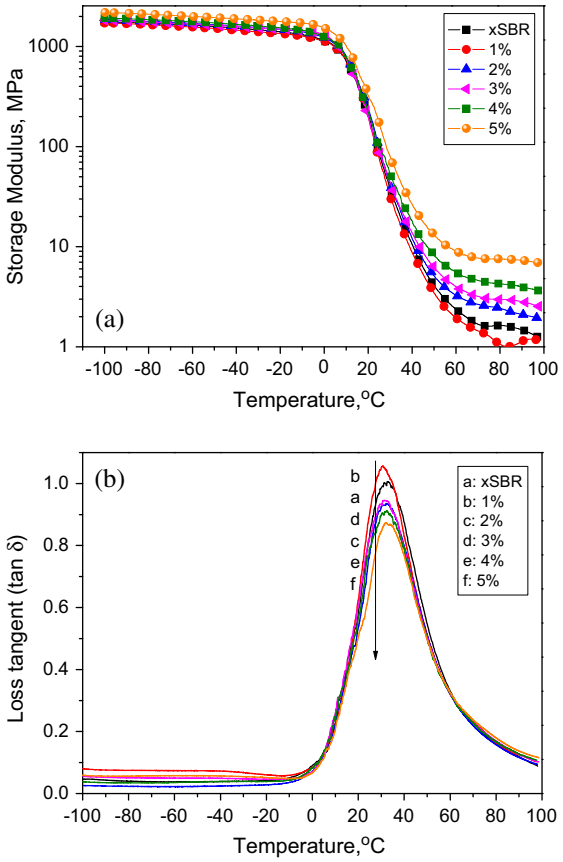

Fig. 11. The temperature dependence of the storage modulus (E') (a) and the loss tangent (tan δ) (b) for xSBR/CNCs nanocomposites with different CNCs contents.

Table 2
The data of storage modulus and loss tangent (tan δ) for xSBR/CNCs nanocomposites.

CNCs content (phr)	Storage modulus at −100 °C (MPa)	Storage modulus at 30 °C (MPa)	Storage modulus at 80 °C (MPa)	tan δ peak values (–)	tan δ peak temperature (°C)
0	1768.4	38.2	1.6	1.01	32.7
1	1718.9	31.5	1.1	1.06	30.8
2	1854.0	41.8	2.4	0.94	32.1
3	1823.5	43.7	3.0	0.95	31.5
4	1924.3	51.7	4.3	0.91	32.3
5	2184.3	80.4	7.5	0.88	32.2

nanocomposite with 5 wt.% CNCs at −100, 30, and 80 °C are measured up to 2184.3, 80.4, and 7.5 MPa which is 23.5%, 110.5% and 368.8% higher than those of neat rubber respectively. This reinforcement trend is consistent with the results from the static tensile tests. The storage modulus of polymer composite is greatly influenced by the formed filler networks in polymer matrix. Therefore, the excellent improvement of E' especially at the rubbery state should be attributed to the percolation networks of CNCs which leads to efficient load transfer from the rubber matrix to the fillers. The relatively low reinforcing effect of CNCs to xSBR at glassy state may be due to the weak molecular mobility ability at this state.

Generally, the glass transition temperature (T_g) of polymer shifted to higher temperature after incorporation of nano-fillers, because nano-fillers hinder the segmental motion of polymer chain segments. However, this disciplinary experience does not take effect in the present study. As shown in Fig. 11(b) and Table 2, the T_g of the materials is the range of 30.8 °C to 32.7 °C. The pure xSBR show the highest T_g of 32.7 °C. The hydroxyl groups on the CNCs surface can form hydrogen bonds with the carboxyl groups in xSBR molecular as illustrated above. This may act as an internal plasticization which results in the shifting of T_g to a lower temperature upon the addition of CNCs [40]. However, further study is still needed to investigate the essential reason for this particular phenomenon. No significant broadening of the tan δ peak is observed in Fig. 11(b). Finally, the peak value of tan δ curve falls dramatically from 1.01 to 0.88 as the concentration of CNCs increases except the 1% CNCs nanocomposite. This is ascribed to the decrease of matrix material amount, which is responsible for damping properties. In previous reports, the decreased peak value in the composites has also been found [37].

3.6. Water response of the mechanical properties of the xSBR/CNCs nanocomposites

The hydrophilic polysaccharide nanocrystals can form percolation network in different polymer matrix, which makes the composite with adaptive mechanical properties. To illustrate the influence of the CNCs on the water response of the mechanical property for xSBR, the modulus of the swollen composites were determined. Fig. 12 shows the tensile moduli of xSBR/CNCs nanocomposites for dry state, equilibrium swelling in deionized water, or swelling to saturation in deionized water followed by redrying. Table 3 summarizes the data of modulus and their changes before and after swelling. The neat xSBR has Young's modulus of 14.1 MPa, which linearly increases with the loading of the CNCs. For the nanocomposite with the highest CNCs content investigated (5 wt.%) a maximum Young's modulus of 39.2 MPa is measured, which represents a

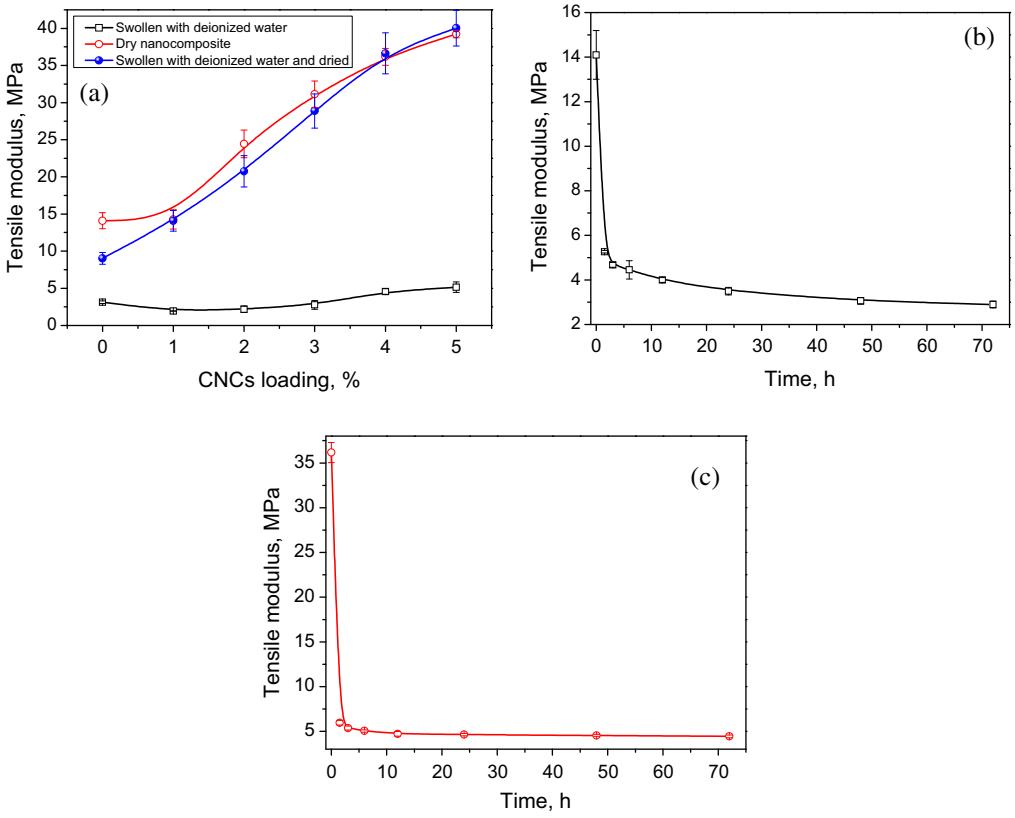

Fig. 12. The tensile moduli of xSBR/CNCs nanocomposites as a function of CNCs loading in the dry state, water-swollen state, and redrying state after swollen (a); the change of tensile modulus as a function of the immersing time upon placing the pure xSBR (b) and xSBR/CNCs nanocomposites with 4 wt.% CNCs (c) films in an aqueous environment.

Table 3
The tensile modulus change for xSBR/CNCs nanocomposites before and after swollen in deionized water (the data in the bracket is the standard deviation).

CNCs content (phr)	Modulus in swollen state (MPa)	Modulus in dry state (MPa)	Change (%)	Modulus of swollen and dried again (MPa)	Recovery ratio (%)
0	3.13 (0.16)	14.10 (1.09)	450.48	9.02 (0.78)	63.97
1	1.94 (0.02)	14.27 (1.30)	735.57	14.09 (1.40)	98.74
2	2.17 (0.43)	24.45 (1.87)	1126.73	20.76 (2.11)	84.91
3	2.76 (0.59)	31.13 (1.78)	1127.90	28.89 (2.31)	92.80
4	4.55 (0.38)	36.17 (1.13)	794.95	36.64 (2.76)	101.30
5	5.14 (0.70)	39.23 (0.49)	763.23	40.03 (2.39)	102.04

stiffness increase of 1.78-fold compared with neat xSBR. The interfacial interactions (hydrogen bonding) between the xSBR and CNCs and the formation of filler network contribute to the increase of the modulus. The moduli at 100% strain also have a similar increasing trend (date not shown). The significant reinforcement effect of the CNCs to xSBR suggests the formation of a percolating CNCs network especially at relatively high CNCs content within the rubbery matrix via the hydrogen bonding interactions between the nanocrystals.

Fig. 12 also shows the tensile moduli of the neat xSBR and xSBR/CNCs nanocomposite that had been immersed in deionized water for 3 days (i.e., to equilibrium). The tensile testing experiments were conducted immediately to avoid the water evaporation. As can be seen from Fig. 12 and Table 3, all the swollen samples exhibit pronounced decreased modulus. The neat xSBR shows a modest decrease ratio of the tensile modulus (450.5%), which is due to that there is not the hydrophilic filler network in the matrix. The greatest mechanical contrast is seen in the case of the nanocomposite, for example, the tensile modulus of the xSBR nanocomposite with 3 wt.% CNCs reduced from 31.13 to 2.76 MPa upon equilibrium swelling. Also, the swelling with water of the composites with 3 wt.% CNCs results in a significant decrease of the tensile strength from 9.16 to 0.94 MPa. The water-responsive mechanical property results are strongly influenced by sample composition, network structure, and the drying conditions. CNCs serve as channels for water absorption and transport within the xSBR matrix and as switchable reinforcing filler of the polymers. After redrying of the swollen samples, the tensile testing was performed again. It can be seen that the nanocomposite samples can almost completely recover to their initial strength and modulus. However, the unfilled xSBR only recovered 63.97% of its original modulus. The CNCs can play the role of the physical crosslinking points via the interfacial hydrogen bonds in the xSBR composite systems [7]. The CNCs networks make the xSBR molecules chains can recovery their initial state due to the crosslinking. Therefore, CNCs can improve the mechanical properties recovery after redrying the swollen sample.

To demonstrate the dynamics of the softening of the nanocomposites upon immersion of the water, the mechanical properties of the sample before and after swollen were established. Fig. 12(b) and (c) show the change of tensile modulus upon placing the pure xSBR and 4 wt.% CNCs films in an aqueous environment, respectively. As expected, it can be seen that the tensile modulus decreased significantly as a function of the immersing time. A stimuli-responsive behavior, i.e. decrease in modulus, is observed for the nanocomposite samples; whereas for pure xSBR samples this is less evident. The percentage decrease in tensile modulus that occurs within the initial 3 h (relative to the modulus at dry state) is 85.17% for the nanocomposite and 66.85% for the pure xSBR sample. The water responses of the mechanical properties are of course strongly influenced by sample composition and the film thickness (here ~300 μm). The higher response rate of the mechanical properties for the xSBR/CNCs nanocomposites is attributed to the disengagement of the percolating CNCs network [41]. The water-triggered modulus changes of the xSBR/CNCs nanocomposites suggest that they are stimuli-responsive polymer composites with adaptive mechanical properties.

3.7. Swelling properties of the xSBR/CNCs nanocomposites

The influence of the CNCs on the water absorption of xSBR was investigated by the water uptake experiment. Fig. 13(a) compares the water swelling ratio of the xSBR/CNCs nanocomposite with different CNCs content. Neat xSBR has a water absorption ratio of 34.1%. All the composites show increased water uptake ratio compared with neat xSBR, which is attributed to the incorporation of the hydrophilic nanocrystals. The water uptake ratio of the nanocomposite increases with the increase in CNCs content up to 2 wt.%. For example, the water uptake at equilibrium of the nanocomposites with 2 wt.% CNCs is 73.4%. Further addition of CNCs (i.e., >3 wt.%) brings slightly decrease in the water uptake ratio. This is possibly attributed to the increased crosslinking density of the xSBR by the nanocrystals [42]. The photographs of dissolution/swell experiment are shown in Fig. 13(b). It can be seen that after swelling both the pure xSBR and the composite rubber turn into white from the transparent color due to the absorption of water. Also, the solution for the nanocomposite with 4 wt.% CNCs is totally transparent, suggesting no dissolution or leaching of CNCs in water. The rigid CNCs networks at high loading within the polymer matrix resulting from three-dimensional hydrogen bonding lead to the slightly decreased water uptake ratio. The absolute value of the water uptake ratio of the composites is higher than that of neat xSBR. However, the decreased water uptake and the diffusion coefficient of water of the polymers by the incorporation of the polysaccharide nanocrystals were found in other reports [43]. This difference may arise from the different polymer matrix.

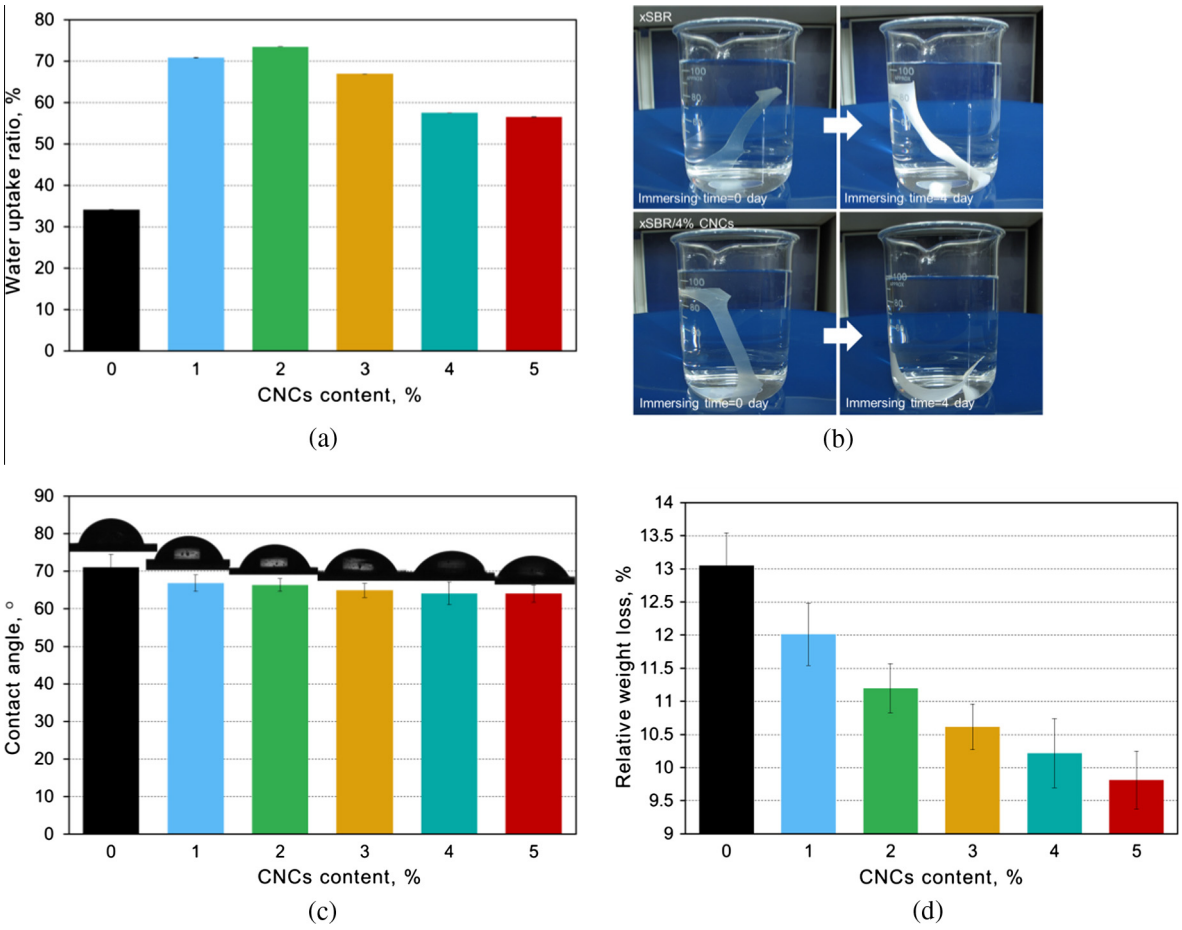

Fig. 13. Water uptake ratios (a), the appearance before and after immersing the water (b), the water contact angle (c), and the relative weight loss in toluene (d) of xSBR/CNCs nanocomposites.

The water contact angles of the pure xSBR and xSBR/CNCs nanocomposite films were also measured to compare the hydrophilicity of the films surface. The results are shown in Fig. 13(c). It can be seen that the water contact angle of the nanocomposites decreases from 71° for neat xSBR film to 64° for the nanocomposite film of the 5 wt.% CNCs. This can be attributed to the slightly increased wettability of the nanocomposite films by the hydrophilic CNCs.

The xSBR/CNCs nanocomposites were immersed in toluene for 72 h, dried for 12 h at 60 °C, and weighed. The fraction of xSBR dissolved in toluene after 72 h were determined, and data are compared in Fig. 13(d). Data show that about 13% of the unfilled xSBR is dissolved in toluene. The dissolution of a limited amount of the rubber is ascribed to the fact that the experiment was performed at room temperature without any stirring [44]. The relative weight loss (RWL) of the xSBR nanocomposites decreases with increase in the CNCs content. For example, about 3% decreases is found for the nanocomposites with 5 wt.% CNCs. The decreased RWL also suggests the increase in the fraction of bonded matrix (FBM) of the nanocomposites, as the bonded rubber on the CNCs cannot be dissolved in the toluene. It could also be due to the formation of rigid chitin networks of the CNCs in the rubber matrix for the CNCs filled rubber materials. However, the influence of this network on the dissolution of rubber chains is limited. The process involves the interfacial interactions between CNCs and the matrix which should be sufficiently strong to prevent the dissolution of rubber chains and maintain them in the "gel" fraction of the sample.

4. Conclusions

Rod-like CNCs are prepared by acid hydrolysis and characterized with various methods. A good dispersion of CNCs aqueous dispersion is obtained by ultrasonic treatment. CNCs has the diameter of ~15 nm and length of 200–500 nm. The addition of CNCs into the xSBR does not influence the transparency of the films. FTIR results show that hydrogen bonding interactions occur between the rubber and the CNCs. CNCs can significantly increase the tensile strength, tensile modulus, and strain at break of xSBR. The xSBR nanocomposite with 3 wt.% CNCs, the tensile strength and the elongation at break is

9.16 MPa and 396%, respectively, which is 123% and 11% higher than those for neat xSBR film. Overloading the CNCs leads to further increased tensile strength and modulus but lowed strain at break. When the content of CNCs is above 3 wt.%, the (020) plane diffraction of CNCs appears in the composite. The dispersion of CNCs is homogenous in the matrix even with the high loadings. The tensile storage moduli of the composites increase with the addition of CNCs except for the nanocomposite with 1% CNCs especially at the rubber region. The T_g of xSBR nearly do not change by the incorporation of the CNCs. A dramatic reduction of tensile modulus is observed for the composite upon submersion in deionized water, for example, the E' of the xSBR nanocomposite with 3 wt.% CNCs reduced from 31.13 to 2.76 MPa upon equilibrium swelling. All the properties change is interpreted as the formation of filler network in the xSBR matrix and the interfacial interactions between CNCs and xSBR. The nanocomposites show increased water uptake ratio and decreased relative weight loss in toluene compared with neat xSBR. The prepared high-performance xSBR/CNCs nanocomposite with adaptive mechanical properties shows potential applications in high performance elastic materials and smart material areas.

Acknowledgments

This work was financially supported by the National Natural Science Foundation of China (Grant Nos. 51473069 and 81171459), and the Guangdong Natural Science Funds for Distinguished Young Scholar (Grant No. S2013050014606), and the Key Project of Department of Education of Guangdong Province (No. CXZD1015).

References

[1] S.J. Eichhorn, Cellulose nanowhiskers: promising materials for advanced applications, Soft Matter 7 (2) (2011) 303–315.
[2] J.-B. Zeng, Y.-S. He, S.-L. Li, Y.-Z. Wang, Chitin whiskers: an overview, Biomacromolecules 13 (1) (2012) 1–11.
[3] D. Klemm, F. Kramer, S. Moritz, T. Lindstrom, M. Ankerfors, D. Gray, A. Dorris, Nanocelluloses: a new family of nature-based materials, Angew. Chem.-Int. Ed. 50 (24) (2011) 5438–5466.
[4] X. Wu, C. Lu, H. Xu, X. Zhang, Z. Zhou, Biotemplate synthesis of polyaniline@ cellulose nanowhiskers/natural rubber nanocomposites with 3D hierarchical multiscale structure and improved electrical conductivity, ACS Appl. Mater. Interf. 6 (23) (2014) 21078–21085.
[5] X. Zhang, X. Wu, C. Lu, Z. Zhou, Dialysis-free and in situ doping synthesis of polypyrrole@cellulose nanowhiskers nanohybrid for preparation of conductive nanocomposites with enhanced properties. ACS Sustain. Chem. Eng. (2015), http://dx.doi.org/10.1021/sc500853m.
[6] N. Lin, J. Huang, P.R. Chang, D.P. Anderson, J.H. Yu, Preparation, modification, and application of starch nanocrystals in nanomaterials: a review, J. Nanomater. 2011 (2011) 20.
[7] J.R. Capadona, K. Shanmuganathan, D.J. Tyler, S.J. Rowan, C. Weder, Stimuli-responsive polymer nanocomposites inspired by the sea cucumber dermis, Science 319 (5868) (2008) 1370–1374.
[8] K. Shanmuganathan, J.R. Capadona, S.J. Rowan, C. Weder, Bio-inspired mechanically-adaptive nanocomposites derived from cotton cellulose whiskers, J. Mater. Chem. 20 (1) (2010) 180–186.
[9] R. Rusli, K. Shanmuganathan, S.J. Rowan, C. Weder, S.J. Eichhorn, Stress-transfer in anisotropic and environmentally adaptive cellulose whisker nanocomposites, Biomacromolecules 11 (3) (2010) 762–768.
[10] J. Mendez, P.K. Annamalai, S.J. Eichhorn, R. Rusli, S.J. Rowan, E.J. Foster, C. Weder, Bioinspired mechanically adaptive polymer nanocomposites with water-activated shape-memory effect, Macromolecules 44 (17) (2011) 6827–6835.
[11] J. Sriupayo, P. Supaphol, J. Blackwell, R. Rujiravanit, Preparation and characterization of alpha-chitin whisker-reinforced poly(vinyl alcohol) nanocomposite films with or without heat treatment, Polymer 46 (15) (2005) 5637–5644.
[12] X. Li, X. Li, B. Ke, X. Shi, Y. Du, Cooperative performance of chitin whisker and rectorite fillers on chitosan films, Carbohyd. Polym. 85 (4) (2011) 747–752.
[13] A.J. Uddin, M. Fujie, S. Sembo, Y. Gotoh, Outstanding reinforcing effect of highly oriented chitin whiskers in PVA nanocomposites, Carbohyd. Polym. 87 (1) (2012) 799–805.
[14] P. Wongpanit, N. Sanchavanakit, P. Pavasant, T. Bunaprasert, Y. Tabata, R. Rujiravanit, Preparation and characterization of chitin whisker-reinforced silk fibroin nanocomposite sponges, Eur. Poly. J. 43 (10) (2007) 4123–4135.
[15] M. Rinaudo, Chitin and chitosan: properties and applications, Progr. Poly. Sci. 31 (7) (2006) 603–632.
[16] M. Mincea, A. Negrulescu, V. Ostafe, Preparation, modification, and applications of chitin nanowhiskers: a review, Rev. Adv. Mater. Sci. 30 (3) (2012) 225–242.
[17] R.H. Marchessault, F.F. Morehead, N.M. Walter, Liquid crystal systems from fibrillar polysaccharides, Nature 184 (4686) (1959) 632–633.
[18] K. Gopalan Nair, A. Dufresne, Crab shell chitin whisker reinforced natural rubber nanocomposites. 1. Processing and swelling behavior, Biomacromolecules 4 (3) (2003) 657–665.
[19] K. Gopalan Nair, A. Dufresne, Crab shell chitin whisker reinforced natural rubber nanocomposites. 2. Mechanical behavior, Biomacromolecules 4 (3) (2003) 666–674.
[20] K. Gopalan Nair, A. Dufresne, A. Gandini, M.N. Belgacem, Crab shell chitin whiskers reinforced natural rubber nanocomposites. 3. Effect of chemical modification of chitin whiskers, Biomacromolecules 4 (6) (2003) 1835–1842.
[21] M. Paillet, A. Dufresne, Chitin whisker reinforced thermoplastic nanocomposites, Macromolecules 34 (19) (2001) 6527–6530.
[22] Y. Lu, L. Weng, L. Zhang, Morphology and properties of soy protein isolate thermoplastics reinforced with chitin whiskers, Biomacromolecules 5 (3) (2004) 1046–1051.
[23] A. Morin, A. Dufresne, Nanocomposites of chitin whiskers from riftia tubes and poly(caprolactone), Macromolecules 35 (6) (2002) 2190–2199.
[24] P.M. Visakh, M. Monti, D. Puglia, M. Rallini, C. Santulli, F. Sarasini, S. Thomas, J.M. Kenny, Mechanical and thermal properties of crab chitin reinforced carboxylated SBR composites, Exp. Poly. Lett. 6 (5) (2012) 396–409.
[25] A. Villares, C. Moreau, I. Capron, B. Cathala, Chitin nanocrystal-xyloglucan multilayer thin films, Biomacromolecules 15 (1) (2014) 188–194.
[26] M. Liu, J. Huang, B. Luo, C. Zhou, Tough and highly stretchable polyacrylamide nanocomposite hydrogels with chitin nanocrystals, Int. J. Biol. Macromol. 78 (2015) 23–31.
[27] A.-R. Mahdavian, M. Abdollahi, Investigation into the effect of carboxylic acid monomer on particle nucleation and growth in emulsifier-free emulsion copolymerization of styrene-butadiene-acrylic acid, Polymer 45 (10) (2004) 3233–3239.
[28] Y. Tang, Y. Li, G. Xue, Y. Zhao, X. Zhang, Y. Zhang, Effect of carboxylated styrene-butadiene rubber latex amount on the viscoelastic behavior of paper coating modified with nanosized particles, Adv. Mater. Res. 236–238 (2011) 1322–1325.
[29] Y. Fan, H. Fukuzumi, T. Saito, A. Isogai, Comparative characterization of aqueous dispersions and cast films of different chitin nanowhiskers/nanofibers, Int. J. Biol. Macromol. 50 (1) (2012) 69–76.
[30] H. Kargarzadeh, I. Ahmad, I. Abdullah, A. Dufresne, S.Y. Zainudin, R.M. Sheltami, Effects of hydrolysis conditions on the morphology, crystallinity, and thermal stability of cellulose nanocrystals extracted from kenaf bast fibers, Cellulose 19 (3) (2012) 855–866.

[31] X. Dong, J.-F. Revol, D. Gray, Effect of microcrystallite preparation conditions on the formation of colloid crystals of cellulose, Cellulose 5 (1) (1998) 19–32.
[32] A. Dufresne, Polysaccharide nano crystal reinforced nanocomposites, Can. J. Chem.-Rev. Canad. Chim. 86 (6) (2008) 484–494.
[33] M. De Sarkar, P.P. De, A.K. Bhowmick, Diimide reduction of carboxylated styrene-butadiene rubber in latex stage, Polymer 41 (3) (2000) 907–915.
[34] Y. Lu, Q. Sun, X. She, Y. Xia, Y. Liu, J. Li, D. Yang, Fabrication and characterisation of a-chitin nanofibers and highly transparent chitin films by pulsed ultrasonication, Carbohyd. Poly. 98 (2) (2013) 1497–1504.
[35] J. Jin, P. Hassanzadeh, G. Perotto, W. Sun, M.A. Brenckle, D. Kaplan, F.G. Omenetto, M. Rolandi, A biomimetic composite from solution self-assembly of chitin nanofibers in a silk fibroin matrix, Adv. Mater. 25 (32) (2013) 4482–4487.
[36] I. Sakurada, Y. Nukushina, T. Ito, Experimental determination of the elastic modulus of crystalline regions in oriented polymers, J. Poly. Sci. 57 (165) (1962) 651–660.
[37] S. Wu, T. Lin, B. Guo, Elastic-resilience-induced dispersion of carbon nanotubes: a novel way of fabricating high performance elastomer, Nanotechnology 24 (46) (2013). 465708.
[38] Y.-W. Cho, J. Jang, C.R. Park, S.-W. Ko, Preparation and solubility in acid and water of partially deacetylated chitins, Biomacromolecules 1 (4) (2000) 609–614.
[39] N. Bitinis, R. Verdejo, J. Bras, E. Fortunati, J.M. Kenny, L. Torre, M.A. López-Manchado, Poly (lactic acid)/natural rubber/cellulose nanocrystal bionanocomposites part I. Processing and morphology, Carbohyd. Poly. 96 (2) (2013) 611–620.
[40] X. Cao, C. Xu, Y. Liu, Y. Chen, Preparation and properties of carboxylated styrene-butadiene rubber/cellulose nanocrystals composites, Carbohyd. Poly. 92 (1) (2013) 69–76.
[41] P.K. Annamalai, K.L. Dagnon, S. Monemian, E.J. Foster, S.J. Rowan, C. Weder, Water-responsive mechanically adaptive nanocomposites based on styrene-butadiene rubber and cellulose nanocrystals—processing matters, ACS Appl. Mater. Interf. 6 (2) (2014) 967–976.
[42] C. Zhou, Q. Wu, Y. Yue, Q. Zhang, Application of rod-shaped cellulose nanocrystals in polyacrylamide hydrogels, J. Colloid Interf. Sci. 353 (1) (2011) 116–123.
[43] Y. Wang, X. Cao, L. Zhang, Effects of cellulose whiskers on properties of soy protein thermoplastics, Macromol. Biosci. 6 (7) (2006) 524–531.
[44] K.G. Nair, A. Dufresne, Crab shell chitin whisker reinforced natural rubber nanocomposites. 1. Processing and swelling behavior, Biomacromolecules 4 (3) (2003) 657–665.